



# The influence of the substrate temperature on the growth mechanism of amine- and thiol-based plasma polymers: A comparative study

Nathan Vinx<sup>1</sup>  | Philippe Leclère<sup>2</sup> | Claude Poleunis<sup>3</sup> | Arnaud Delcorte<sup>3</sup> | Pierre Mathieu<sup>1</sup> | Damien Cossement<sup>4</sup> | Rony Snyders<sup>1,4</sup> | Damien Thiry<sup>1</sup> 

<sup>1</sup>Chimie des Interactions Plasma-Surface (ChIPS), Institut Matériaux, Université de Mons, Mons, Belgium

<sup>2</sup>Laboratoire de Physique des Nanomatériaux et Energie (LPNE), Institut Matériaux, Université de Mons, Mons, Belgium

<sup>3</sup>Bio- and Soft Matter (BSMA), Institute of Condensed Matter and Nanosciences (IMCN), Université catholique de Louvain, Louvain-la-Neuve, Belgium

<sup>4</sup>Materia Nova Research Center, Mons, Belgium

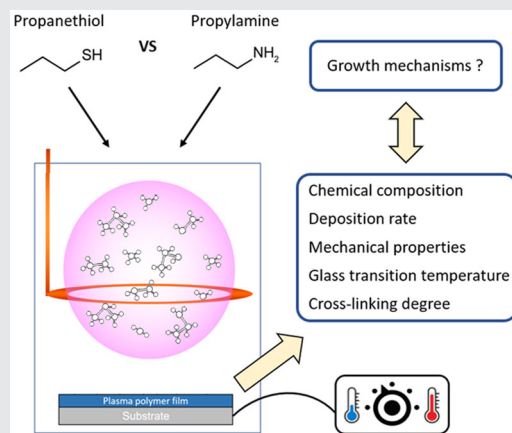
## Correspondence

Damien Thiry, Chimie des Interactions Plasma-Surface (ChIPS), Université de Mons, 20 Pl du Parc, Mons B-7000, Belgium.

Email: [Damien.Thiry@umons.ac.be](mailto:Damien.Thiry@umons.ac.be)

## Abstract

This work aims to provide new insights into the link between the growth mechanisms of functionalized plasma polymer films (PPFs) and the substrate temperature ( $T_S$ ). By means of AFM-based techniques, it has been demonstrated that the mechanical behavior of the coatings is dramatically affected by  $T_S$  and the precursor employed (i.e., 1-propanethiol or 1-propylamine). While propylamine-based PPFs behave as hard elastic materials regardless of  $T_S$ , propanethiol-based PPFs evolve from viscous liquids to elastic solids with increasing  $T_S$ . This behavior can be understood considering the glass transition temperature of PPF. For both precursors, the latter is correlated to the cross-linking density controlled through the energy density brought by positive ions to the growing film.



## KEYWORDS

growth mechanism, plasma polymer, substrate temperature

## 1 | INTRODUCTION

For more than 40 years, functionalized plasma polymer films (PPFs) exhibiting reactive chemical functions, such as  $-SH$ ,<sup>[1]</sup>  $-NH_2$ ,<sup>[2]</sup>  $-OH$ <sup>[3]</sup>, or  $-COOH$ <sup>[4]</sup> have been widely

studied due to their high applicative potential as for instance the fabrication of biosensors,<sup>[5]</sup> the synthesis of antibacterial coatings,<sup>[6]</sup> or as a support for stabilizing nanoparticles.<sup>[7]</sup>

In brief, the plasma polymerization process consists of the activation of an organic precursor into a plasma

**Abbreviations:**  $NH_2$ -PPF, propylamine-based plasma polymer film; PPF, plasma polymer film; R, deposition rate; SH-PPF, propanethiol-based plasma polymer film; SPM, scanning probe microscopy;  $T_g$ , glass transition temperature; ToF-SIMS, time of flight-secondary ion mass spectrometry;  $T_T$ , surface transition temperature; XPS, X-ray photoelectron spectroscopy.

phase resulting in the formation of reactive species including ions and neutrals. Their subsequent condensation on surfaces exposed to the plasma leads to the formation of the PPF.<sup>[8,9]</sup> Their complex growth mechanism involving numerous surface and gas phase reactions is responsible for the uniqueness of PPF such as the absence of repeating units contrary to conventional polymers as well as their outstanding properties including good thermal stability, insolubility in most solvents, and excellent adhesion properties on a large range of substrates. These properties as well as the industrial scalability of the process justify the increasing interest in the plasma polymerization technique.<sup>[10,11]</sup>

Another advantage of the method is its versatility enabling the modulation of the physicochemical properties (i.e., chemical composition, cross-linking degree) of PPF by a clever choice of the process parameters, paving the way for the fabrication of a tailor-made material for a given application. To date, the energy invested per particle in the discharge controlling the fragmentation of the organic precursor has been the most studied parameter. From these studies, it can be concluded that the use of low energetic conditions results in the deposition of PPF with a higher retention degree of the precursor functionality and a lower cross-linking density.<sup>[12,13]</sup>

In contrast, despite being introduced in the '80s by Yasuda as a critical parameter, the influence of the substrate temperature ( $T_S$ ) governing the adsorption/desorption equilibrium has received little attention. Some antecedent works, mainly related to the growth of C:H and fluorine-based PPF, have revealed a decrease in the deposition kinetics with increasing  $T_S$ .<sup>[14,15]</sup> This trend was explained by the displacement of the adsorption/desorption equilibrium toward desorption with increasing  $T_S$ . Recently, in our group, it has been demonstrated that  $T_S$  also plays a key role in controlling the physicochemical properties of propanethiol-based PPF.<sup>[1,16–18]</sup> Interestingly, it has been shown that the mechanical behavior of the coatings correlated with their glass transition temperature is dramatically affected by  $T_S$ : from a highly viscous liquid to a hard elastic solid (with a rigidity modulus of  $9.94 \pm 5.88$  GPa) for a short range of  $T_S$  variation (i.e., from 10°C to 45°C), opening the door for the design of mechanically responsive PPF of interest for flexible electrodes.<sup>[18–22]</sup> Nevertheless, the fundamental explanation of this unusual behavior in comparison with the dependency of the process with the power is still open to question. Moreover, light must be shed on whether a similar trend will be observed with other plasma polymer families.

In this context, this work aims at providing new insights about the influence of  $T_S$  on the growth mechanism of PPF considering two precursors (i.e., 1-propanethiol and 1-propylamine) presenting a similar hydrocarbon backbone and a different reactive chemical function (i.e., –SH and –NH<sub>2</sub>). For both precursors, a complete characterization of the physicochemical properties of the coatings including their mechanical properties by scanning probe microscopy (SPM), glass transition temperature (time of flight-secondary ion mass spectrometry [ToF-SIMS]), chemical composition (X-ray photoelectron spectroscopy [XPS]), cross-linking density (ToF-SIMS) as well as their growth kinetics (SPM) is undertaken. The obtained data are discussed based on the influence of the precursor and  $T_S$  on the growth mechanism of the plasma polymers.

## 2 | EXPERIMENTAL SECTION

PPFs were grown from 1-propanethiol (98%, Sigma-Aldrich) and 1-propylamine (99%, Sigma-Aldrich) on  $1 \times 1$  cm<sup>2</sup> silicon substrates previously cleaned with isopropanol three times and dried under a nitrogen flow before synthesis.

The PPF synthesis has been carried out in a metallic deposition chamber (65 cm in length and 35 cm in diameter) kept under vacuum by a combination of turbomolecular and primary pumps allowing to reach a residual pressure of  $2 \times 10^{-6}$  Torr. The plasma was sustained by an internal water-cooled one-turn inductive Cu coil (10 cm in diameter) connected to an Advanced Energy radiofrequency (13.56 MHz) power supply via a matching network. The three-dimensional scheme of the deposition chamber can be found elsewhere.<sup>[23]</sup> For all depositions, the precursor flow rate as well the power dissipated into the plasma were fixed to 5 sccm and 40 W, respectively. The distance between the coil and the substrate was 10 cm. A combination of electrical resistances (for heating) and liquid nitrogen (for cooling) coupled with a thermocouple affixed to the substrate holder allowed us to externally control ( $\pm 1^\circ\text{C}$ ) the substrate temperature during the depositions.  $T_S$  was stabilized 30 min before starting the deposition for each experiment, ensuring the thermal equilibrium between the silicon substrate and the substrate holder. Five different temperatures have been investigated in this work:  $T_S = -10, 0, 10, 23, \text{ or } 45^\circ\text{C}$ . The following notation is used in this article to discriminate PPF based on the  $T_S$  at which they were synthesized: PPF synthesized at “X”°C as  $T_S$  from the precursor containing the “–Z” chemical reactive function in its backbone (–NH<sub>2</sub> for propylamine, –SH for propanethiol) is notated Z–PPF<sub>X</sub>°C.

The deposition rates for each precursor have been obtained through atomic force microscopy (AFM) measurements. The PPF surface was scratched with a cutter blade, generating a step between the PPF surface and the substrate surface, giving the coating thickness.

XPS experiments were carried out to evaluate the chemical composition of PPF (i.e., [N]/[C] or [S]/[C]). To avoid excessive surface contamination, after their synthesis, the samples were directly transferred to the instrument. The analyses have been performed using a PHI 5000 VersaProbe apparatus. A monochromatized Al K $\alpha$  line (1486.6 eV) has been used as a photon source. All spectra were charge-corrected with respect to the hydrocarbon component of the C1s peak at 285 eV. For spectral curve fitting of the high-resolution carbon photoelectron peaks, using MultiPak software, a FWHM of 1.1–1.4 eV and a Gauss–Lorentz function (70% Gauss) were applied.

ToF-SIMS measurements have been carried out to characterize the evolution of the PPF cross-linking degree with  $T_S$  for each precursor. The analyses were performed directly after the synthesis of the PPF. Static ToF-SIMS data have been recorded in positive mode using a ToF-SIMS IV instrument supplied by ION TOF GmbH. A pulsed Ar<sup>+</sup> 10 keV ion beam (0.75 pA) rastered over a scan area of 300  $\times$  300  $\mu\text{m}^2$  in 125 s at least five times per sample.

The PPF surface glass transition temperatures have been determined by ToF-SIMS measurements applying a method described elsewhere.<sup>[24]</sup> Static ToF-SIMS data have been acquired in positive mode using a ToF-SIMS<sup>[5]</sup> instrument provided by ION TOF GmbH, used both as a sputtering and analytical source. The instrument is fitted with an Ar gas cluster ion beam (Ar-GCIB) working at 10 keV during the analyses. The Ar cluster distribution was centered on Ar<sub>3000</sub><sup>+</sup>. An AC target current of 0.037 pA with a bunched pulse width around 70 ns was used on a raster of 128  $\times$  128 data points over an area of 500  $\times$  500  $\mu\text{m}^2$ . To avoid the charging effects of the PPF, an electron flood gun ( $E_k = 5$  eV) was used. A special sample holder called “Holder G” supplied by ION TOF GmbH allowed us to control and vary from  $-120^\circ\text{C}$  to  $160^\circ\text{C}$  (the samples’ temperature) during the analyses. The temperature has been stabilized for 20 min before each analysis. A presputtering of  $2 \times 10^{13}$  Ar<sub>3000</sub><sup>+</sup>/cm<sup>2</sup> was conducted in DC mode over an area of 1000  $\times$  1000  $\mu\text{m}^2$  before each analysis to eliminate all potential surface contaminations.

The analysis of the mechanical properties was conducted by AFM using a Bruker Icon Dimension instrument, equipped with a Nanoscope V controller, using the PeakForce Quantitative Nanomechanical Measurements (QNM) mode. Each force-distance curve acquisition was performed at 2 kHz with an image of 256  $\times$  256 points on a PPF area of 5  $\times$  5  $\mu\text{m}^2$ .

Measurements have been carried out at three different locations on each PPF surface. An RTESPA300-30 tip (Bruker Nano Inc.) was used in this study to enhance the precision of the measurements. The spring constant of the tip, which was equal to 48.97 N/m, was calibrated and provided by the supplier. The deflection sensitivity was calibrated on sapphire, corresponding to  $58.81 \pm 0.60$  nm/V. The tip radii were also provided by Bruker and were found to be equal to 27 nm. The rigidity modulus values were estimated by fitting part of the unloading curve using the Johnson–Kendall–Roberts (JKR) model. This model is suitable for analyzing “soft” materials with a non-negligible adhesion between the tip and the sample surface, including polymers. A detailed description of the equations describing the JKR model can be found elsewhere.<sup>[25]</sup> The thickness of all PPF analyzed was fixed to  $\sim 250$  nm to avoid any influence of the substrate on the JKR rigidity modulus measurement.

## 3 | RESULTS AND DISCUSSION

### 3.1 | Results

#### 3.1.1 | Deposition kinetics

The evolution of the deposition rates ( $R$ ) of PPFs synthesized from propanethiol and propylamine as a function of  $T_S$  is depicted in Figure 1. It should be noted that the deposition rate of SH-PPF at lower  $T_S$  (i.e., 0 and  $-10^\circ\text{C}$ ) could not be accurately evaluated because the liquid nature of the coating makes the scratch procedure difficult. Therefore, additional points for  $T_S$  between  $10^\circ\text{C}$  and  $45^\circ\text{C}$  have been measured to evaluate

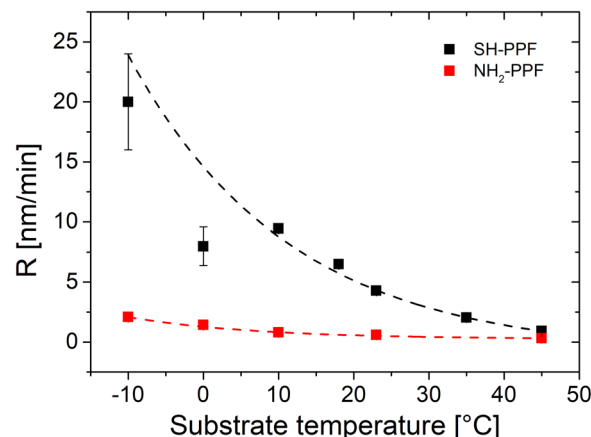


FIGURE 1 Evolution of the deposition rate ( $R$ ) of plasma polymer film (PPF) with  $T_S$ .

the dependence of the deposition kinetics with  $T_S$  with a higher degree of accuracy.

For each PPF family,  $R$  decreases with  $T_S$  (i.e., from  $20 \pm 4$  to  $0.92 \pm 0.02$  nm/min and from  $2.08 \pm 0.02$  to  $0.32 \pm 0.01$  nm/min for SH-PPF and  $\text{NH}_2$ -PPF, respectively) according to an exponential law (dashed lines on Figure 1), in accordance with the results observed in the literature for different PPF families.<sup>[26,27]</sup>

Besides, for a given  $T_S$ , the deposition rate of SH-PPF is significantly higher than for  $\text{NH}_2$ -PPF, suggesting different growth mechanisms. This point will be discussed later (see in Section 3.2).

### 3.1.2 | Mechanical properties

The mechanical properties of  $\text{NH}_2$ -PPF synthesized for  $T_S$  between  $-10^\circ\text{C}$  and  $23^\circ\text{C}$  have been probed with the Peak-Force QNM method.<sup>[28]</sup> This technique allows the characterization of the elastic behavior of the material through the evaluation of its rigidity modulus. Briefly, the rigidity modulus of a material can be associated with its Young modulus for which elasticity tensors are not considered. It should be noted that the  $\text{NH}_2$ -PPF<sub>45°C</sub> was not analyzed as 14 hours of deposition were required to obtain an adequate thickness avoiding any influence of the substrate on the measurement, which was too long to ensure the stability of  $T_S$  during the whole synthesis.

The recorded force–distance curves were fitted with the JKR theory as already applied to other PPFs.<sup>[18,25]</sup> Following this procedure, Gaussian-shaped distributions of the calculated rigidity modulus values were obtained. The mean modulus is assumed to be the center of the gaussian distribution, associated with the full width at half-maximum (FWHM) as a confidence interval. An example of a mechanical properties mapping, a typical force–distance curve, and a Gaussian distribution of the rigidity modulus for  $\text{NH}_2$ -PPF<sub>10°C</sub> is presented in Supporting Information (Figure S1). The RMS roughness of all PPF being lower than 0.5 nm, the rigidity modulus measurements are assumed to be independent of the PPF topography.<sup>[29]</sup>

As plotted in Figure 2, the rigidity modulus of  $\text{NH}_2$ -PPF increases (i.e., from  $2.17 \pm 0.49$  to  $13.83 \pm 3.42$  GPa) with  $T_S$  before reaching a plateau (i.e.,  $13.58 \pm 2.52$  GPa for  $\text{NH}_2$ -PPF<sub>23°C</sub>). These values are in line with the typical ones generally reported in the literature for PPF.<sup>[30]</sup>

Regarding the SH-PPF, as shown in our previous work, the samples can be discriminated into two categories: PPF synthesized at (i) higher  $T_S$  (i.e.,  $\geq 23^\circ\text{C}$ ) and (ii) lower  $T_S$  (i.e.,  $\leq 10^\circ\text{C}$ ).<sup>[18]</sup> The former ones have also been analyzed by Peak-Force QNM following the

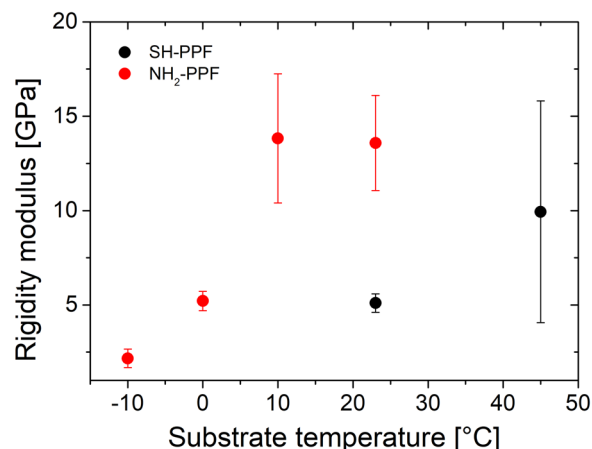


FIGURE 2 Evolution of the rigidity modulus of SH-PPF (black marks) and  $\text{NH}_2$ -PPF (red marks) as a function of  $T_S$ .

same data treatment as for  $\text{NH}_2$ -PPF. It can be observed that the rigidity modulus increases from  $5.1 \pm 0.49$  to  $9.94 \pm 5.88$  GPa when  $T_S$  increases from  $23^\circ\text{C}$  to  $45^\circ\text{C}$  (Figure 2).

For  $T_S \leq 10^\circ\text{C}$ , the shape of the recorded approach–retract curve makes any mathematical treatment to extract the mechanical parameters impractical (see Supporting Information: Figure S2).<sup>[18]</sup> From our previous study investigating the relaxation dynamic of a scratch induced on the PPF surface with the AFM tip, it was concluded that, for  $T_S = 10^\circ\text{C}$ , the material behaves as a viscous liquid with a viscosity of about  $10^6$  Pa.s.<sup>[18]</sup> While further decreasing  $T_S$ , the velocity of the scratch recovery makes impossible any reliable measurements of the relaxation dynamic by AFM, likely due to an even lower viscosity (see Supporting Information: Figure S3).

From the analysis of the PPF mechanical properties, it can be concluded that, for both precursors, the general trend is an increase in the rigidity of the PPF with  $T_S$ . For the same  $T_S$ , SH-PPF is always softer than  $\text{NH}_2$ -PPF. While SH-PPF evolves from a liquid to a (visco)elastic solid with  $T_S$ ,  $\text{NH}_2$ -PPF remains elastic regardless of  $T_S$ . Thus, the impact of  $T_S$  on the PPF mechanical properties is more pronounced on SH-PPF than on  $\text{NH}_2$ -PPF.

### 3.1.3 | Glass transition temperature

Considering conventional polymerization, the mechanical properties of polymers synthesized from the same monomer can vary, evolving from a liquid to an elastic solid, as a function of their glass transition temperature.<sup>[31]</sup> Therefore, the evaluation of  $T_g$  can inform on the mechanical properties of the materials. Recently, Poleunis et al. have developed a ToF-SIMS-based method

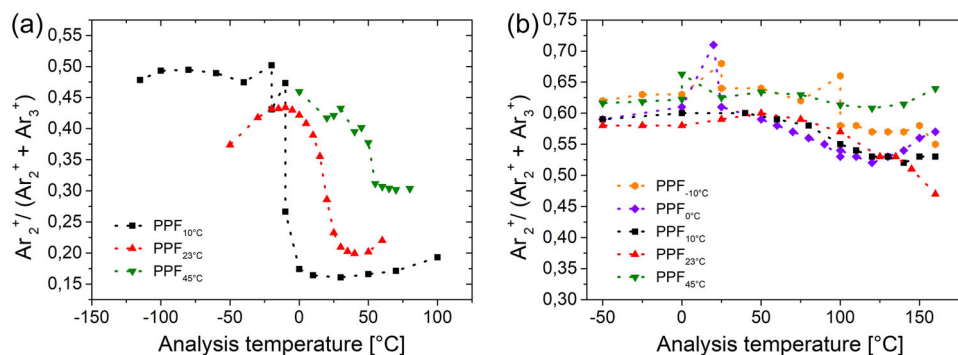


FIGURE 3  $Ar_2^+ / (Ar_2^+ + Ar_3^+)$  ratio of backscattered ions collected during time of flight-secondary ion mass spectrometry experiments versus the analysis temperature for (a) SH-PPF and (b)  $NH_2$ -PPF.

allowing the evaluation of the polymer glass transition temperature, including thin films.<sup>[24]</sup> Briefly, the method consists of measuring the rate of backscattered  $Ar_n^+$  ions from  $Ar_{3000}^+$  cluster during ToF-SIMS measurements carried out on samples at different analysis temperatures. They found out that the  $Ar_2^+ / (Ar_2^+ + Ar_3^+)$  ratio dramatically evolves at a temperature close to their  $T_g$  as evaluated by conventional differential scanning calorimetry. This ratio follows a sigmoidal trend as a function of the analysis temperature. The temperature corresponding to the inflexion point is named *transition temperature* ( $T_T$ ) of the materials and is directly correlated to the glass transition temperature ( $T_g$ ).<sup>[24]</sup> This method has been applied to SH-PPF and  $NH_2$ -PPF to evaluate their transition temperature.

As shown in Figure 3a, all recorded curves for SH-PPF exhibit a sigmoid shape, in agreement with the literature. The  $T_T$  of SH-PPF<sub>10 $^{\circ}C$</sub> , SH-PPF<sub>23 $^{\circ}C$</sub> , and SH-PPF<sub>45 $^{\circ}C$</sub>  have been found to be  $-10^{\circ}C$ ,  $18^{\circ}C$ , and  $52^{\circ}C$ , respectively (Figure 4). These values correlate with the previously discussed AFM measurements carried out at room temperature ( $T_{room}$ ). From these data, it has been shown that for a  $T_T \ll T_{room}$  (i.e., PPF<sub>10 $^{\circ}C$</sub> ), the PPF demonstrates a viscous behavior whereas for  $T_T \geq T_{room}$  (i.e., PPF<sub>23 $^{\circ}C$</sub> ), the PPF exhibits (visco)elastic properties. Finally, for  $T_T \gg T_{room}$  (i.e., PPF<sub>45 $^{\circ}C$</sub> ), the PPF behaves as an elastic solid. As for the evaluation of the mechanical properties, SH-PPFs synthesized at  $T_S \leq 0^{\circ}C$  were not suitable for this analysis.

Regarding  $NH_2$ -PPF, none of the experimental curves exhibit a sigmoid shape (Figure 3b). All curves present a “plateau” with the analysis temperatures. Consequently,  $T_T$  could not be deduced within the range of  $T_S$  considered here (i.e.,  $-120^{\circ}C$  to  $160^{\circ}C$ ). The transition temperatures of  $NH_2$ -PPF are probably out of the analysis temperature range probed here (i.e.,  $>160^{\circ}C$ ). This is supported by the investigation of the mechanical

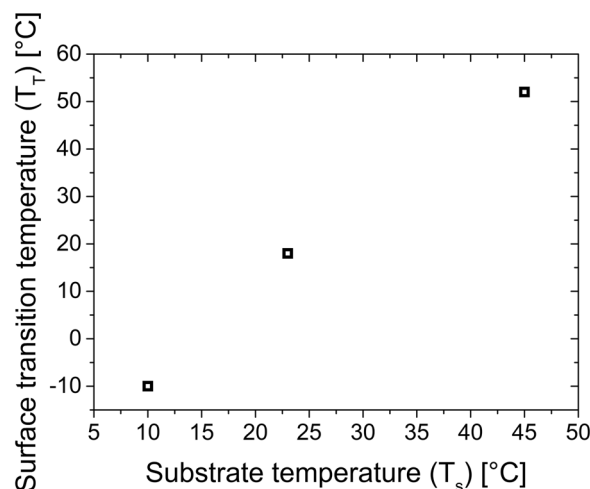


FIGURE 4 Evolution of the  $T_T$  of the SH-PPF evaluated by time of flight-secondary ion mass spectrometry as a function of  $T_S$ .

properties of  $NH_2$ -PPF. Indeed, these PPFs behave like hard elastic solids, indicating that the temperature at which the mechanical properties were probed ( $T_{room}$ ) is lower than their  $T_T$ .

### 3.1.4 | Cross-linking degree and chemical composition

It is well-known, in the context of conventional polymers, that both mechanical properties and  $T_g$  are dramatically affected by the cross-linking degree and the chemical composition of the polymeric network.<sup>[32–35]</sup> Based on these considerations, the evolution of the cross-linking degree and the chemical composition of PPF with  $T_S$  has been evaluated by means of additional ToF-SIMS measurements and XPS, respectively.

It has been shown that the cross-linking degree of PPF is inversely correlated to the total yields of secondary

ions collected ( $\Sigma_{SI}$ ) for ToF-SIMS spectra recorded in positive mode.<sup>[36]</sup>

As presented in Figure 5,  $\Sigma_{SI}$  decreases with  $T_S$ , revealing an increase in the cross-linking degree for both  $NH_2$ - and SH-PPF.

Regarding the  $NH_2$ -PPF, the observed trend in Figure 5 correlates with the evolution of the rigidity modulus measured by AFM for  $-10^\circ C < T_S < 23^\circ C$ . Surprisingly,  $\Sigma_{SI}$  decreases from  $NH_2$ -PPF<sub>10°C</sub> to  $NH_2$ -PPF<sub>23°C</sub>, and is not correlated, in this case, to an increase in the rigidity modulus (i.e., plateau at  $\sim 13.5$  GPa). This behavior has already been observed in the case of ethyl lactate-based PPFs for which the increase in the cross-linking density of the coatings was correlated to an increase in the hardness while the Young modulus remains stable.<sup>[30]</sup>

Concerning the SH-PPF, the increase in the cross-linking density with  $T_S$  reduces the mobility of the molecular segments accompanied by an increase in  $T_T$ . A critical value of the cross-linking degree for  $10^\circ C < T_S < 23^\circ C$  is probably reached, inducing a mechanical transition from liquid to solid similar to the gelation of conventional polymers.<sup>[34]</sup>

It is important to note that the cross-linking density between SH-PPF and  $NH_2$ -PPF cannot be discriminated based on  $\Sigma_{SI}$  as the total yield of secondary ions is dependent on the chemical composition of the probed surface. However, based on the mechanical behavior of SH-PPF at low  $T_S$  (i.e., highly viscous liquid) in comparison with  $NH_2$ -PPF (i.e., hard elastic solid) and their  $T_T$  (from  $-10^\circ C$  to  $52^\circ C$  for SH-PPF and  $>160^\circ C$  for  $NH_2$ -PPF) a much higher cross-linking density for  $NH_2$ -PPF is expected.

The Figure S4 (in Supporting Information) represents typical XPS survey spectra, revealing the presence of carbon, nitrogen, and oxygen for  $NH_2$ -PPF; and carbon,

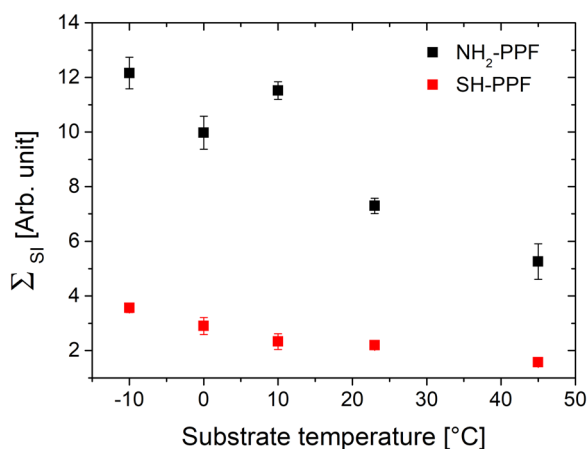


FIGURE 5 Evolution of  $\Sigma_{Secondary\ Ions}$  as a function of  $T_S$ .

sulfur, and oxygen for SH-PPF. The presence of oxygen is ascribed to the reaction between the remaining trapped radicals and oxygen/water present in the ambient air taking place during the transfer of the samples from the deposition chamber to the XPS.<sup>[37–39]</sup>

As presented in Figure 6, the heteroelement to the carbon ratio (i.e.,  $[S]/[C]$  for SH-PPF and  $[N]/[C]$  for  $NH_2$ -PPF) is higher for SH-PPF than for  $NH_2$ -PPF. Regarding SH-PPF, the  $[S]/[C]$  ratio oscillates between 0.73 and 0.89 for  $-10 < T_S < 23^\circ C$  before decreasing to 0.55 for PPF<sub>45°C</sub>. It should be emphasized that for each SH-PPF, the  $[S]/[C]$  ratio is higher than the value found in the precursor (i.e., 0.33, dashed gray line in Figure 6). Although this behavior is quite unusual for PPF synthesized from precursors with other heteroelements, this is in line with our previous studies dedicated to sulfur-based PPF.<sup>[16,17]</sup> This can be explained by the presence of  $H_2S$  trapped species in the matrix during the PPF synthesis; the amount of trapped molecules being dependent on the thermal conditions during the growth.<sup>[1]</sup> As shown in our previous work, these trapped species acting as plasticizers tend to reduce the glass transition temperature of the PPF synthesized at low  $T_S$ .<sup>[18]</sup>

In contrast, the  $[N]/[C]$  ratio of  $NH_2$ -PPF is similar regardless of  $T_S$  (i.e., around 0.27) taking into account the confidence intervals (Figure 6). Interestingly, this ratio is also lower than the precursor one (i.e., 0.33), in concordance with the literature.<sup>[2]</sup> The lower  $[X]/[C]$  ratio compared to the SH-PPF one does not suggest the trapping of nitrogen-based stable molecules in the plasma polymer network.

Owing to the numerous reactions occurring in a plasma, a large variety of N-containing groups are created and incorporated into the PPF. However, from

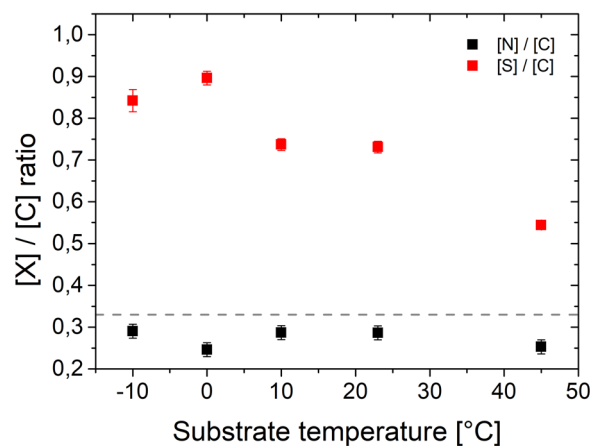


FIGURE 6 Evolution of the  $[S]/[C]$  (for propanethiol-based PPF, red marks) and  $[N]/[C]$  (for propylamine-based PPF, black marks) ratios as a function of  $T_S$ .

the  $[N]/[C]$  ratio, no information can be extracted concerning the nature of the chemical bonds involving N and C with  $T_S$ . Therefore, the envelope of the C1s peak from XPS spectra has been fitted into fourth components namely C1, C2, C3, and C4 referred as carbon-carbon/hydrogen bonds (C-C/H) at 284.8 eV, amines (C-NR with R=H or C) and imines (C=N) bonds at 285.6 eV, nitriles (C≡N), ethers and alcohols (C-OR with R=H or C) functions at 286.6 eV and carbonyl groups (C=O) at 288 eV, respectively.<sup>[40,41]</sup> A typical example of the high-resolution C1s envelope spectral curve fitting is illustrated in Figure 7a. It should be noted that a similar data treatment cannot be applied for SH-PPF as the chemical shifts associated with the different sulfur-based functionalities (e.g., C-SH, C-S-C, C=S, ...) are too low compared to the XPS resolution for allowing an accurate fitting procedure for the C<sub>1s</sub> peak as well as for the S<sub>2p</sub> one.<sup>[42,43]</sup> As it can be observed in Figure 7b, the relative concentration of the different components remains stable as a function of  $T_S$ , considering a variation of a maximum of 5% of the value independently of  $T_S$ . Besides the overall nitrogen content, we can thus conclude that the chemistry of NH<sub>2</sub>-PPF is unaffected by  $T_S$  and does not influence their  $T_T$  and mechanical properties.

### 3.2 | Discussion

On the basis of the collected data, some important statements have been made regarding the influence of the organic chemical precursor and  $T_S$  on the growth mechanism of the PPF. While  $T_S$  significantly affects the physicochemical properties of propanethiol PPF, for propylamine, it does not.

To understand this behavior, some basics about the growth mechanism have to be detailed. In our conditions, reactive species (mainly radicals and to a lesser extent ions) are created in the plasma by electronic collisions. At the same time, the growing film is continuously bombarded by positive ions (with kinetic energy typically ranging from 10 to 30 eV), inducing chemical bonds breaking at the interface and thus forming surface radical sites.<sup>[8,44]</sup> Therefore, the film-forming species generated in the plasma adsorb at the interface and react with the surface-activated site through the formation of chemical bonds. This is referred to the activated growth model (AGM) developed by d'Agostino in the 1980s.<sup>[10,15]</sup>

Based on this approach, the deposition rate ( $R$ ) is proportional to the flux of film-forming species toward the interface ( $F_R$ ) and the density of surface reactive sites ( $S_R$ ):

$$R \sim F_R S_R, \quad (1)$$

now, if we go deeper with regard to the interaction of the film-forming species with the interface, it can be considered that, at first, the reactive moieties are physisorbed in a “weakly adsorbed state” and then diffuse before reaching a surface radical and then form a chemical bond through a surface recombination reaction.<sup>[45]</sup> On this basis, the residence time ( $\tau$ ), in other words, the meantime that the particles spend on a surface is crucial for the chemical incorporation of the film-forming species. Indeed, increasing (decreasing)  $\tau$  results in a higher (lower) probability for the reactive species to find a chemisorption site before being desorbed. Taking into account this statement, Equation (1) can be rewritten as:

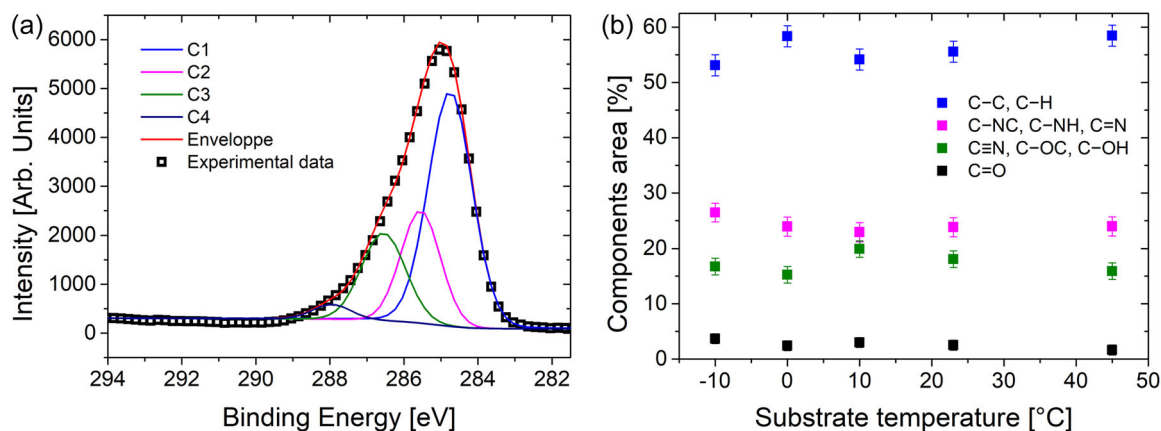


**FIGURE 7** (a) Typical spectral curve fitting of high-resolution C1s carbon photoelectron peak for NH<sub>2</sub>-PPF<sub>10°C</sub>. (b) Evolution of the C1, C2, C3, and C4 components relative area of the high-resolution C1s peak for NH<sub>2</sub>-PPF as a function of  $T_S$ .

$$R \sim F_R \cdot S_R \cdot \tau, \quad (2)$$

actually,  $\tau$  is defined according to Equation (3)<sup>[1]</sup>:

$$\tau = \tau_0 \cdot e^{-E_{\text{phys}}/kT_s}, \quad (3)$$

where  $\tau_0$ ,  $E_{\text{phys}}$ , and  $k$  correspond to the lowest possible residence time (i.e., the inverse of the vibrational frequency of the surface bond,  $\sim 10^{-12}$ – $10^{-13}$  s), the physisorption energy, and the Boltzmann constant, respectively.

Then, inserting Equation (3) into Equation (2) gives:

$$R \sim F_R \cdot S_R \cdot \tau_0 \cdot e^{-E_{\text{phys}}/kT_s}. \quad (4)$$

From Equation (4), only the exponential term depends on  $T_s$ , explaining the trend observed in Figure 1 based on the deposition kinetics. Indeed,  $F_R$  and  $S_R$  directly depend on the fragmentation degree of the precursor in the plasma and the energy brought by positive ions at the interface, respectively.<sup>[8,15,46]</sup>

Plotting  $\ln(R)$  as a function of  $1/T_s$ , therefore, gives access to  $E_{\text{phys}}$  for both employed precursors:  $-0.55 \pm 0.06$  eV for SH-PPF and  $-0.25 \pm 0.01$  eV for  $\text{NH}_2$ -PPF (Figure 8), representing typical physisorption values of adsorbed species on a given surface.<sup>[47–49]</sup>  $E_{\text{phys}}$  can be viewed as apparent physisorption energy for the overall growth process, specific to a precursor and the experimental conditions. It corresponds to the activation energy for the thermal desorption of the film-forming species when adsorbing in a “weakly adsorbed state”.<sup>[45]</sup> The more exothermic  $E_{\text{phys}}$  obtained for SH-PPF contributes to the higher deposition kinetics by increasing the residence time of the film-forming species at the interface and hence the occurrence of a termination reaction with a surface radical site. This also favors the

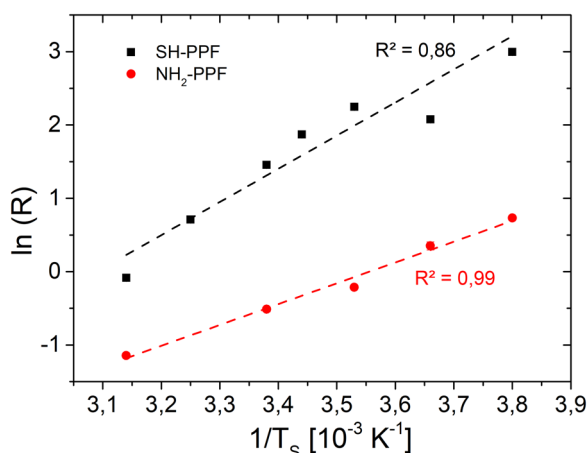


FIGURE 8 Evolution of  $\ln(R)$  as a function of the reverse  $T_s$ .

trapping phenomenon leading to the incorporation of stable species in the polymeric network.<sup>[17,50]</sup>

One possible explanation for the higher  $E_{\text{phys}}$  value for sulfur-based particles is the higher polarizability of sulfur in comparison to nitrogen likely increasing the van der Waals interactions with the surface and hence the physisorption energy.<sup>[51]</sup>

It can be emphasized that for a given PPF family, investigating the deposition rate versus  $T_s$  enables quantitatively extracting important quantities regarding plasma surface interaction. This macroscopic approach of the interface would be complementary to the macroscopic view as developed by Hegemann, enabling the determination of the activation energy of several precursors regarding their dissociation in the plasma by studying the deposition rate as a function of the energy invested per particle.<sup>[52]</sup> Combining both methods would allow us to draw a complete macroscopic view of the plasma polymerization process.

To explain the significant difference between the PPF families in terms of the dependence of their mechanical properties on their growth kinetics, the concept of energy density ( $\varepsilon$ ) has to be introduced.  $\varepsilon$  is defined as the energy brought to the growing film through ionic bombardment and normalized with respect to the total amount of matter deposited according to<sup>[53]</sup>:

$$\varepsilon = \frac{\Gamma_i E_{\text{mean}}}{R}, \quad (5)$$

where  $\Gamma_i$  corresponds to the flux of ions reaching the growing film,  $E_{\text{mean}}$  the mean energy of the bombarding ions, and  $R$  the deposition rate of the PPF. For several plasma polymer families, a linear correlation has been found between the cross-linking degree (directly influencing the mechanical properties) and  $\varepsilon$ .<sup>[13]</sup> Combined with Equation (4),  $\varepsilon$  can be expressed according to:

$$\varepsilon \sim \frac{\Gamma_i E_{\text{mean}}}{F_R \cdot S_R \cdot \tau_0 \cdot e^{-E_{\text{phys}}/kT_s}}. \quad (6)$$

As in our experimental window, only  $T_s$  is varied, it can be rationally assumed that  $\Gamma_i$  and  $E_{\text{mean}}$  (mainly influenced by the plasma parameters, i.e., the electron density and temperature) are identical whatever the precursor. On the other hand, according to Equation (5),  $\varepsilon$  increases for both precursors with  $T_s$  (as  $R$  decreases, see Figure 1), explaining the increase in the cross-linking density of the polymeric network and hence the rigidity of the material. Considering a similar ion flux and mean energy for the bombarding ions in our experimental window, it can be estimated that  $\varepsilon$  increases by a factor of 20 and 7 for SH-PPF and  $\text{NH}_2$ -PPF,



respectively. The larger variation in terms of energy density for propanethiol, due to its higher  $E_{\text{phys}}$  value, could explain the more pronounced impact of  $T_S$  on the cross-linking density of the plasma polymer. Indeed, for  $T_S \leq 10^\circ\text{C}$ , the material behaves as a highly viscous liquid (with  $T_g \leq -10^\circ\text{C}$ ), while for  $T_S \geq 23^\circ\text{C}$  the increase in the cross-linking degree results in the formation of hard elastic PPF (with  $T_g \geq 18^\circ\text{C}$ ). For  $\text{NH}_2$ -PPF, the lower deposition rate values (i.e., higher  $\varepsilon$ ) gives rise for all  $T_S$  conditions to a sufficient cross-linking density for the material to behave as hard elastic solid PPF (with  $T_g > 160^\circ\text{C}$ ).

From Equation (6), it is obvious that  $E_{\text{phys}}$ , strongly influenced by the chemical nature of the precursor, plays a key role in the value of  $\varepsilon$  and hence in the control of the mechanical behavior of the PPF. The higher is  $E_{\text{phys}}$ , the higher the panel of mechanical properties achievable by tuning the substrate temperature.

## 4 | CONCLUSION

In this work, the influence of  $T_S$  on the growth mechanism of plasma polymers prepared from propanethiol and propylamine was investigated through a detailed characterization of their physicochemical properties. As a general trend,  $T_S$  has a more pronounced impact on the growth of SH-PPF in comparison with  $\text{NH}_2$ -PPF. Indeed, the deposition kinetics, the chemical composition, the cross-linking density, the glass transition temperature, and the mechanical properties of the corresponding sulfur-based plasma polymers are significantly affected by  $T_S$ . On the other hand, for  $\text{NH}_2$ -PPF, slight variations of the deposition rate, the cross-linking degree, and the mechanical properties are highlighted.

This discrepancy between both precursors has been understood considering the impact of  $T_S$  on the plasma/surface interaction and specifically on the residence time of the film-forming species at the surface. Indeed, considering the physisorption of the reactive species as a prior step before their chemisorption, their meantime spent at the growing film interface controls the deposition rate. This is supported by the exponential dependence of the deposition kinetics of both plasma polymer families with  $T_S$ . Furthermore, the temperature dependence of the growth kinetics also gives access to the apparent physisorption energy of the film-forming species for both systems revealing a higher adsorption energy for SH-PPF in comparison to  $\text{NH}_2$ -PPF (i.e.,  $-0.55 \pm 0.06$  eV for SH-PPF vs.  $-0.25 \pm 0.01$  eV for  $\text{NH}_2$ -PPF). This highlights the influence of the chemical nature of the molecule source on the plasma/surface

interaction and explains the more pronounced impact of  $T_S$  on the propanethiol plasma polymerization process.

In turn, for a given set of plasma parameters, the modulation of  $T_S$  allows tuning (through the variation of the deposition rate) the energy density brought to the growing film by positive ions. The latter directly influences the cross-linking density of the PPF and hence their mechanical properties revealing the attractiveness of  $T_S$  as a tuning parameter. It is important to highlight that the strategy of modulating the energy load in the plasma as usually employed in the literature results in the increase of both the intensity of the ionic bombardment and the deposition rate in limiting the control on the energy density brought at the interface.

The whole set of our results unambiguously demonstrates the major role played by  $T_S$  on the growth mechanism of functionalized plasma polymers. The investigation of the deposition kinetics versus  $T_S$ , for a given precursor, can also be employed as a tool for quantitatively probing the interaction between the species produced in the plasma and at the interface. This approach is complementary to the already developed macroscopic views investigating the activation kinetics in the plasma and paves the way for a more complete fundamental understanding of the molecular growth mechanism of plasma polymers.

## CONFLICT OF INTEREST STATEMENT

The authors declare no conflict of interest.

## DATA AVAILABILITY STATEMENT

The data that support the findings of this study are available from the corresponding author upon reasonable request.

## ORCID

Nathan Vinx  <http://orcid.org/0009-0002-9370-5052>

Damien Thiry  <http://orcid.org/0000-0001-6703-1512>

## REFERENCES

- [1] D. Thiry, F. J. Aparicio, P. Laha, H. Terryn, R. Snyders, *J. Vac. Sci. Technol. A* **2014**, *32*, 050602.
- [2] C. Vandenabeele, M. Buddhadasa, P.-L. Girard-Lauriault, R. Snyders, *Thin Solid Films* **2017**, *630*, 100.
- [3] L. M. Watkins, A. F. Lee, J. Moir, K. Wilson, *ACS Biomater. Sci. Eng.* **2017**, *3*, 88.
- [4] R. Morent, N. De Geyter, S. Van Vlierberghe, A. Beaurain, P. Dubrue, E. Payen, *Prog. Org. Coat.* **2011**, *70*, 336.
- [5] E. Makhneva, A. Manakhov, P. Skladal, L. Zajičková, *Surf. Coat. Technol.* **2016**, *290*, 116.
- [6] Y. W. Chan, K. S. Siow, P. Y. Ng, U. Gires, B. Yeop Majlis, *Mater. Sci. Eng.: C* **2016**, *68*, 861.

- [7] B. Joseph, N. Ninan, R. M. Visalakshan, C. Denoual, R. Bright, N. Kalarikkal, Y. Grohens, K. Vasilev, S. Thomas, *Compos. Sci. Technol.* **2021**, *202*, 108544.
- [8] D. Thiry, S. Konstantinidis, J. Cornil, R. Snyders, *Thin Solid Films* **2016**, *606*, 19.
- [9] R. Snyders, D. Hegemann, D. Thiry, O. Zabeida, J. Klemberg-Sapieha, L. Martinu, *Plasma Sources Sci. Technol.* **2023**, *32*, 074001.
- [10] H. Biederman, *Plasma Polymer Films*, World Scientific, Singapore, **2004**.
- [11] N. Inagaki, *Plasma Surface Modification and Plasma Polymerization*, CRC Press, Boca Raton, USA, **1996**.
- [12] J. Ryssy, E. Prioste-Amaral, D. F. N. Assuncao, N. Rogers, G. T. S. Kirby, L. E. Smith, A. Michelmores, *Phys. Chem. Chem. Phys.* **2016**, *18*, 4496.
- [13] D. Hegemann, E. Körner, N. Blanchard, M. Drabik, S. Guimond, *Appl. Phys. Lett.* **2012**, *101*, 211603.
- [14] H. Deutsch, H. Kersten, S. Klagge, A. Rutscher, *Contrib. Plasma Phys.* **1988**, *28*, 149.
- [15] R. D'Agostino, F. Cramarossa, F. Fracassi, E. Desimoni, L. Sabbatini, P. G. Zamboni, G. Caporiccio, *Thin Solid Films* **1986**, *143*, 163.
- [16] F. J. Aparicio, D. Thiry, P. Laha, R. Snyders, *Plasma Processes Polym.* **2016**, *13*, 814.
- [17] D. Thiry, F. J. Aparicio, N. Britun, R. Snyders, *Surf. Coat. Technol.* **2014**, *241*, 2.
- [18] N. Vinx, P. Damman, P. Leclère, B. Bresson, C. Fretigny, C. Poleunis, A. Delcorte, D. Cossement, R. Snyders, *D. Thiry, Soft Matter* **2021**, *17*, 10032.
- [19] D. Thiry, N. Vinx, P. Damman, F. J. Aparicio, P. Y. Tessier, D. Moerman, P. Leclère, T. Godfroid, S. Desprez, R. Snyders, *Plasma Processes Polym.* **2020**, *17*, 2000119.
- [20] M. Li, J. Liang, X. Wang, M. Zhang, *Sensors*. **2020**, *20*, 371.
- [21] I. Hopp, A. Michelmores, L. E. Smith, D. E. Robinson, A. Bachhuka, A. Mierczynska, K. Vasilev, *Biomaterials* **2013**, *34*, 5070.
- [22] A. J. S. Ribeiro, Y.-S. Ang, J.-D. Fu, R. N. Rivas, T. M. A. Mohamed, G. C. Higgs, D. Srivastava, B. L. Pruitt, *Proc. Natl. Acad. Sci. USA* **2015**, *112*, 12705.
- [23] D. Thiry, N. Britun, S. Konstantinidis, J.-P. Dauchot, M. Guillaume, J. Cornil, R. Snyders, *J. Phys. Chem. C* **2013**, *117*, 9843.
- [24] C. Poleunis, V. Cristaudo, A. Delcorte, *J. Am. Soc. Mass Spectrom.* **2017**, *29*, 4.
- [25] K. L. Johnson, K. Kendall, A. Roberts, *Proc. R. Soc. A. Math. Phys. Sci.* **1971**, *324*, 301.
- [26] H. Yasuda, C. Wang, *J. Polym. Sci., Part A: Polym. Chem.* **1985**, *23*, 87.
- [27] T. B. Casserly, K. K. Gleason, *Chem. Vap. Deposition* **2006**, *12*, 59.
- [28] A. Kwaśniewska, M. Świetlicki, A. Prószyński, G. Gładyszewski, *Polymers* **2021**, *13*, 244.
- [29] P. Trtik, J. Kaufmann, U. Volz, *Cem. Concr. Res.* **2012**, *42*, 215.
- [30] S. Ligot, E. Bousser, D. Cossement, J. Klemberg-Sapieha, P. Viville, P. Dubois, R. Snyders, *Plasma Processes Polym.* **2015**, *12*, 508.
- [31] V. R. Gowariker, N. Viswanathan, J. Sreedhar, *Polymer Science*, New Age International, New Delhi, India **1986**.
- [32] K. Bandzierz, L. Reuvekamp, J. Dryzek, W. Dierkes, A. Blume, D. Bielinski, *Materials* **2016**, *9*, 607.
- [33] K. L. Ngai, *Physical Properties of Polymers*, 3rd ed., Cambridge University Press, Cambridge, **2004**.
- [34] H. H. Winter, F. Chambon, *J. Rheol.* **1986**, *30*, 367.
- [35] M. K. Mundra, C. J. Ellison, P. Rittigstein, J. M. Torkelson, *Eur. Phys. J.: Spec. Top.* **2007**, *141*, 143.
- [36] D. Cossement, F. Renaux, D. Thiry, S. Ligot, R. Francq, R. Snyders, *Appl. Surf. Sci.* **2015**, *355*, 842.
- [37] T. R. Gengenbach, Z. R. Vasic, S. Li, R. C. Chatelier, H. J. Griesser, *Plasmas and Polym.* **1997**, *2*, 91.
- [38] T. R. Gengenbach, H. J. Griesser, *J. Polym. Sci., Part A: Polym. Chem.* **1998**, *36*, 985.
- [39] T. R. Gengenbach, Z. R. Vasic, R. C. Chatelier, H. J. Griesser, *J. Polym. Sci., Part A: Polym. Chem.* **1994**, *32*, 1399.
- [40] M. Buddhadasa, P.-L. Girard-Lauriault, *Thin Solid Films* **2015**, *591*, 76.
- [41] D. Thiry, A. Chauvin, A. A. El Mel, C. Cardinaud, J. Hamon, E. Gautron, N. Stephant, A. Granier, P. Y. Tessier, *Plasma Processes Polym.* **2017**, *14*, 1700042.
- [42] E. Kasperek, D. Thiry, J. R. Tavares, M. R. Wertheimer, R. Snyders, P. L. Girard-Lauriault, *Plasma Processes Polym.* **2018**, *15*, 1800036.
- [43] D. Thiry, R. Francq, D. Cossement, D. Guerin, D. Vuillaume, R. Snyders, *Langmuir*. **2013**, *29*, 13183.
- [44] D. Thiry, F. Reniers, R. Snyders, *Surface Modification of Polymers: Methods and Applications*, Wiley, Hoboken, USA **2019**, p. 67.
- [45] A. von Keudell, *Plasma Sources Sci. Technol.* **2000**, *9*, 455.
- [46] J. Friedrich, *Plasma Processes Polym.* **2011**, *8*, 783.
- [47] M. Scheffler, C. Stampfl, *Electron. Struct.* **2000**, *2*, 286.
- [48] A. S. Raman, A. Vojvodic, *Handbook of Materials Modeling: Applications: Current and Emerging Materials*, Springer, New York, USA **2020**, p. 1321.
- [49] B. A. De Moor, M.-F. Reyniers, G. B. Marin, *Phys. Chem. Chem. Phys.* **2009**, *11*, 2939.
- [50] D. Thiry, R. Francq, D. Cossement, M. Guillaume, J. Cornil, R. Snyders, *Plasma Processes Polym.* **2014**, *11*, 606.
- [51] R. H. S. Winterton, *Contemp. Phys.* **1970**, *11*, 559.
- [52] D. Hegemann, *J. Phys. D: Appl. Phys.* **2013**, *46*, 205204.
- [53] D. Hegemann, U. Schütz, E. Körner, *Plasma Processes Polym.* **2011**, *8*, 689.

## SUPPORTING INFORMATION

Additional supporting information can be found online in the Supporting Information section at the end of this article.

**How to cite this article:** N. Vinx, P. Leclère, C. Poleunis, A. Delcorte, P. Mathieu, D. Cossement, R. Snyders, D. Thiry, *Plasma Process. Polym.* **2023**, e2300138. <https://doi.org/10.1002/ppap.202300138>